

Optoelectronic oscillator-based interrogation system for Michelson interferometric sensors

Ling Liu(刘玲), Xiaoyan Wu(吴小龑), Guodong Liu(刘国栋), Tigang Ning(宁提纲), Jian Xu(许建), and Haidong You(油海东)

Citation: Chin. Phys. B, 2022, 31 (**9**): 090702. DOI: 10.1088/1674-1056/ac4f59
Journal homepage: http://cpb.iphy.ac.cn; http://iopscience.iop.org/cpb

What follows is a list of articles you may be interested in

Numerical study of a highly sensitive surface plasmon resonance sensor based on circular-lattice holey fiber

Jian-Fei Liao(廖健飞), Dao-Ming Lu(卢道明), Li-Jun Chen(陈丽军), and Tian-Ye Huang(黄田野)
Chin. Phys. B, 2022, 31 (**6**): 060701. DOI: 10.1088/1674-1056/ac43a5

A stopping layer concept to improve the spatial resolution of gas-electron-multiplier neutron detector

Jianjin Zhou(周建晋), Jianrong Zhou(周健荣), Xiaojuan Zhou(周晓娟), Lin Zhu(朱林), Jianqing Yang(杨建清), Guian Yang(杨桂安), Yi Zhang(张毅), Baowei Ding(丁宝卫), Bitao Hu(胡碧涛), Zhijia Sun(孙志嘉), Limin Duan(段利敏), and Yuanbo Chen(陈元柏)
Chin. Phys. B, 2022, 31 (**5**): 050702. DOI: 10.1088/1674-1056/ac398e

Finite element simulation of Love wave sensor for the detection of volatile organic gases

Yan Wang(王艳), Su-Peng Liang(梁苏鹏), Shu-Lin Shang(商树林),Yong-Bing Xiao(肖勇兵), and Yu-Xin Yuan(袁宇鑫)
Chin. Phys. B, 2022, 31 (**3**): 030701. DOI: 10.1088/1674-1056/ac3ec9

Effect of staggered array structure on the flow field of micro gas chromatographic column

Daohan Ge(葛道晗), Zhou Hu(胡州), Liqiang Zhang(张立强), and Shining Zhu(祝世宁)
Chin. Phys. B, 2022, 31 (**1**): 010701. DOI: 10.1088/1674-1056/ac0902

A modified analytical model of the alkali-metal atomic magnetometer employing longitudinal carrier field

Chang Chen(陈畅), Yi Zhang(张燚), Zhi-Guo Wang(汪之国), Qi-Yuan Jiang(江奇渊), Hui Luo(罗晖), and Kai-Yong Yang(杨开勇)
Chin. Phys. B, 2021, 30 (**5**): 050707. DOI: 10.1088/1674-1056/abd7d3

Optoelectronic oscillator-based interrogation system for Michelson interferometric sensors

Ling Liu(刘玲)[1], Xiaoyan Wu(吴小龑)[2,3,†], Guodong Liu(刘国栋)[2,3], Tigang Ning(宁提纲)[1], Jian Xu(许建)[1], and Haidong You(油海东)[4]

[1] *Key Laboratory of All Optical Network and Advanced Telecommunication Network, Ministry of Education, Institute of Lightwave Technology, Beijing Jiaotong University, Beijing* 100044, *China*

[2] *Institute of Fluid Physics, China Academy of Engineering Physics, Mianyang* 621900, *China*

[3] *Key Laboratory of Science and Technology on High Energy Laser, China Academy of Engineering Physics, Mianyang* 621900, *China*

[4] *Qingdao Agricultural University, Qingdao* 266109, *China*

(Received 2 November 2021; revised manuscript received 2 January 2022; accepted manuscript online 27 January 2022)

High-performance interrogation systems for optical fiber sensors are extensively required for environmental condition monitoring applications. In this article, we propose and demonstrate a Michelson interferometer (MI) interrogation system based on an optoelectronic oscillator (OEO). The frequency of the OEO is related to the free spectral range (FSR) of the MI. Thus, when the FSR of the MI varies with a change in external physical factors, the frequency of the OEO shifts and can be used for interrogation. We demonstrate that the temperature sensitivity and interrogation resolution are 35.35 MHz/°C and 0.012 °C, respectively. Such an OEO-based scheme enables wavelength-to-frequency mapping and promises a wide linear interrogation range, high resolution and high-speed interrogation.

Keywords: interrogation system, optical fiber sensor, optoelectronic oscillator

PACS: 07.07.Df, 32.30.Bv, 84.40.–x **DOI:** 10.1088/1674-1056/ac4f59

1. Introduction

Optical fiber sensors, with their advantages of light weight, compact size and immunity to electromagnetic interference, have been widely used in the diagnosis and monitoring of environmental conditions.[1–4] Among the various optical fiber sensors, the Michelson interferometer (MI), with its merits of ease of fabrication and high sensitivity, has applications in aeronautics, perimeter protection, bridge security monitoring and environmental condition monitoring.[5–8] However, MIs are conventionally interrogated by wavelength interrogation or Fourier transform, which requires an optical spectrum analyzer (OSA).[5] Therefore the interrogation resolution and speed are largely limited by the OSA; these limitations would in turn affect the performance of the sensing and measurement systems.

An interrogation scheme enabled by electrical approaches therefore has potential in applications requiring high resolution and high-speed interrogation. Generally, electrical domain-based interrogation of a MI can be implemented using the following three approaches. The first approach is based on intensity interrogation and is achieved by monitoring the power of the electrical signal output by a photodetector (PD). This is a simple approach. However, the linear interrogation range is limited by the small linear region of the interference fringe.[9] In addition, the interrogation accuracy would suffer from power fluctuations. The second approach, phase-generated carrier-based interrogation, is achieved by monitoring the phase difference between the two signals transmitted in the two arms of the MI. A wide linear interrogation range and real-time interrogation can be enabled. Nevertheless, additional phase modulation of the reference signal is required,[6] increasing the complexity of the interrogation system. The third approach uses microwave photonic technologies, which convert the wavelength shift in the optical domain into a frequency shift in the electrical domain. For example, MI interrogation systems based on a periodic microwave photonic filter (MPF) have been proposed for temperature measurement[7] and displacement measurement,[8] but the use of a vector network analyzer (VNA) makes the system costly.

In this paper, we propose an interrogation system for a MI sensor. An optoelectronic oscillator (OEO), enabled by the sinusoidal nature of the MI interference fringe and a single-passband MPF, are incorporated in the proposed interrogation system. The central frequency of the single-passband MPF, determined by the dispersive characteristics of the employed dispersive medium and the free spectral range (FSR) of the MI, mainly determine the frequency of the OEO. When the sensing arm of the MI is affected by the external physical factors to be measured, the interference fringe of the MI (i.e., the FSR) would shift, leading to a frequency shift of the single-passband MPF and ultimately the OEO. Such wavelength-to-frequency mapping therefore allows interrogation of the MI by tracking the frequency shift of the OEO. We also use a fiber ring resonator (FRR) for fine mode selection of the OEO,

†Corresponding author. E-mail: wuxiaoyan1219@sina.cn

© 2022 Chinese Physical Society and IOP Publishing Ltd

which further contributes to the stability of the OEO and the interrogation accuracy of the proposed interrogation system. Our proposed scheme brings high-performance interrogation with a wide linear range, high resolution and high speed, and can be used in applications in bridge security monitoring and industrial machinery sensing that require the measurement of strain or temperature.

2. Principle of operation

A schematic diagram of our proposed interrogation system is illustrated in Fig. 1. A homemade erbium-doped fiber amplifier (EDFA) is used as the broadband optical source (BOS) to provide a broadband optical signal with a full bandwidth of 60 nm. After transmission through a MI with two unbalanced arms, a sinusoidal broadband optical signal is obtained and then sent to a phase modulator (PM). After amplification in another EDFA and transmission through a dispersive medium (i.e., a dispersion-compensating fiber, DCF), the modulated signal is transmitted through a FRR and then converted into a radio-frequency (RF) signal in a PD. The generated RF signal is amplified by an electrical amplifier (EA) and then divided into two paths via a divider. One path of the RF signal is fed back to the PM to form the OEO loop while the other is monitored via an electrical spectrum analyzer (ESA).

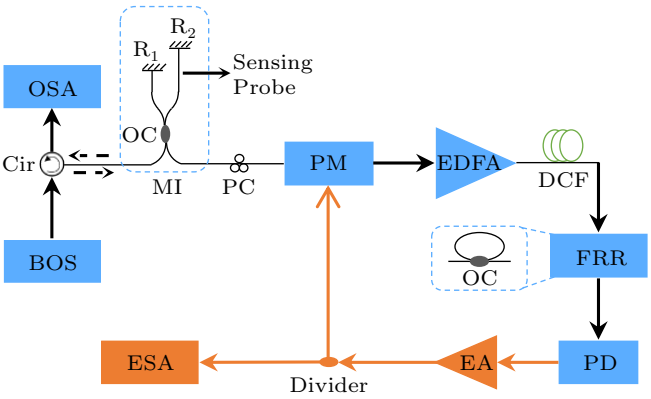


Fig. 1. The proposed OEO-based interrogation system with the optical path shown in black and the electrical path shown in orange. BOS, broadband optical source; Cir, circulator; OSA, optical spectrum analyzer; OC, optical coupler; R_i, in-line reflector ($i = 1, 2$); MI, Michelson interferometer; PC, polarization controller; PM, phase modulator; EDFA, erbium-doped fiber amplifier; DCF, dispersion-compensating fiber; FRR, fiber ring resonator; PD, photodetector; EA, electrical amplifier; ESA, electrical spectrum analyzer.

The interrogation principle is described below. The transmission function of the MI can be written as

$$T(\lambda) \propto \cos\left(\frac{2\pi n \Delta L}{\lambda}\right), \tag{1}$$

where λ is the wavelength of the broadband optical signal, n is the refractive index of the optical fiber composing the MI, ΔL is the length difference between the two arms of the MI. The FSR of the MI can be derived as $\Delta\lambda_{\mathrm{FSR}} = \lambda^2/2n\Delta L$. Thus, the sinusoidal broadband optical signal with a FSR equal to $\Delta\lambda_{\mathrm{FSR}}$ is obtained.

As reported in Mora *et al.*,[10] a single-passband MPF can be obtained by the joint operation of the sinusoidal broadband optical signal, an electro-optic modulator, a dispersive medium and a PD. The central frequency of the single-passband MPF can be written as[10]

$$f_{\mathrm{MPF}} = -\frac{1}{D\Delta\lambda_{\mathrm{FSR}}}, \tag{2}$$

where D is the total dispersion (ps/nm) of the DCF (and is fixed in this work). Hence, f_{MPF} is uniquely linearly proportional to $\Delta\lambda_{\mathrm{FSR}}$. Similar to the mechanism of the optical fiber laser,[11] if the single-passband MPF alone is incorporated in a closed OEO loop and provides sufficient gain for the OEO loop, a RF signal whose frequency is equal to f_{MPF} would be obtained. Considering the 3-dB bandwidth of the single-passband MPF and the single-mode oscillation of the OEO further, we used a FRR composed of an optical coupler and a length of optical fiber in our work. This introduces an additional infinite impulse response (IIR)-MPF with a periodic response and narrow bandwidth nature for each peak. The FSR of the FRR-based IIR-MPF can be expressed as[12,13]

$$\Delta f_{\mathrm{FRR}} = \frac{c}{nL_{\mathrm{FRR}}}, \tag{3}$$

where L_{FRR} is the length of the optical fiber constituting the FRR, and c is the speed of light in a vacuum. Therefore, in this work, the open-loop response of the proposed OEO (i.e., the MPF response) would be determined jointly by the responses of the single-passband MPF and the FRR-based IIR-MPF. The frequency of the OEO is mainly determined by f_{MPF} and is uniquely linearly proportional to $\Delta\lambda_{\mathrm{FSR}}$. The mode spacing of the OEO is jointly affected by the FSR of the FRR-based IIR-MPF and the length L_{DCF} of the DCF.[13] Thereby, the wavelength-to-frequency mapping from the FSR $\Delta\lambda_{\mathrm{FSR}}$ of the MI to the frequency of the OEO is established.

When the sensing arm of the MI is affected by external physical factors, the optical spectrum at the output of the MI would shift, leading to the variation of $\Delta\lambda_{\mathrm{FSR}}$. For temperature measurement, the varied FSR of the MI can be written as

$$\Delta\lambda'_{\mathrm{FSR}} = \frac{\lambda^2}{2n\Delta L + 2(\alpha+\xi)nL\Delta T}, \tag{4}$$

where α and ξ are the thermal expansion coefficient of the optical fiber and the thermo-optic coefficient, respectively, L is the length of the optical fiber affected by the temperature variation and ΔT is the temperature variation. Thanks to the wavelength-to-frequency mapping, the frequency of the OEO shifts in correspondence with $\Delta\lambda_{\mathrm{FSR}}$. The frequency shift of the OEO therefore can be derived as

$$\Delta f = \left|\frac{1}{D\Delta\lambda'_{\mathrm{FSR}}} - \frac{1}{D\Delta\lambda_{\mathrm{FSR}}}\right| = \frac{1}{D\lambda^2}(\alpha+\xi)\cdot 2nL\Delta T. \tag{5}$$

It can be found that the frequency shift of the OEO is linearly proportional to the variation of temperature when the total dispersion D of the DCF is fixed. In a similar way, the linear relationship between the variation of strain $\Delta\varepsilon$ and the frequency shift of the OEO can be expressed as $\Delta f = (1-p_e)2nL\Delta\varepsilon/D\lambda^2$, where p_e is the effective elastic-optic coefficient of the fiber. Hence, interrogation of the MI can be implemented by monitoring the frequency shift of the OEO.

3. Experimental results and discussion

The experimental setup of the proposed interrogation system is shown in Fig. 1. A homemade EDFA with non-uniform spontaneous emission spectrum profile acts as the BOS. As observed by the OSA (Yokogawa, AD6370D) and shown in Fig. 2(a), a sinusoidal broadband optical signal with a $\Delta\lambda_{FSR}$ of 0.406 nm @ 1540 nm is obtained by the joint use of the BOS and the MI. Then, the sinusoidal broadband optical signal is modulated in the PM (Thorlabs, LN53S-FC) with a 3-dB bandwidth of 10 GHz and a half-wave voltage of 3.5 V. The DCF has a total dispersion D of -334 ps/nm and a length L_{DCF} of around 2.4 km. After transmission through the DCF and amplification by another EDFA (Lion, BROADTRAN-16), the modulated optical signal is sent to the FRR, which comprises a 40:60 optical coupler and an optical fiber with a length L_{FRR} ($\sim$ 500 m). Finally, the optical signal is converted into a RF signal in the PD (Thorlabs, RXM25AF) and amplified by an EA with a 3-dB bandwidth of 20 GHz and a typical gain of 26 dB. The generated oscillation signal is monitored by the ESA (Agilent, N9010A).

Joint operation of the sinusoidal broadband optical signal with $\Delta\lambda_{FSR} = 0.406$ nm and a DCF with $D = -334$ ps/nm leads to a single-passband MPF and the OEO, the responses of which are shown in Fig. 2(b). The frequencies of the single-passband MPF and the OEO are in good agreement, although they are slightly different from the theoretical result based on Eq. (2). This frequency difference is mainly introduced by the instability of the MI reflection spectrum and the resulting measurement error of $\Delta\lambda_{FSR}$. However, it would not greatly deteriorate the performance of the proposed interrogation system since the interrogation is not performed by tracking the wavelength shift. The 3-dB bandwidth of the single-passband MPF is around 396 MHz, which would lead to severe mode competition in the OEO. The FRR-based IIR-MPF is therefore introduced to mitigate this problem. The zoom-in spectrum of the OEO is shown in Fig. 3. Multiple modes with a spacing of 84 kHz and 429 kHz are observed simultaneously; the former is determined by c/nL_{DCF}, and the latter is determined by Δf_{FRR}. It worth noting that, due to the FRR, single-mode oscillation of the OEO is guaranteed. A BOS with Gaussian or rectangular profile can also be used to narrow the 3-dB bandwidth of the single-passband MPF and mitigate the mode competition to some extent.

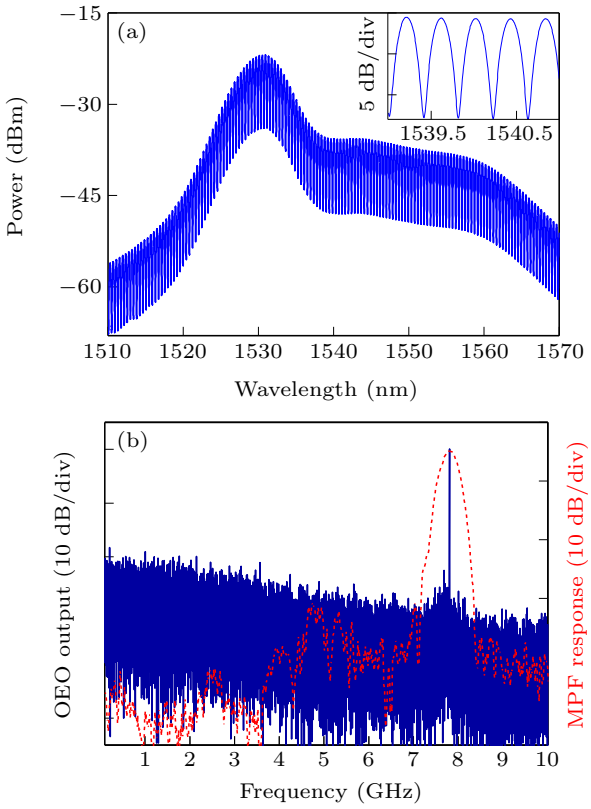


Fig. 2. (a) Optical spectrum of the sinusoidal broadband optical signal measured at the output of the MI. Inset: zoomed-in view of the optical spectrum. (b) Measured OEO output (blue solid curve) and the single-passband MPF response (red short dash curve).

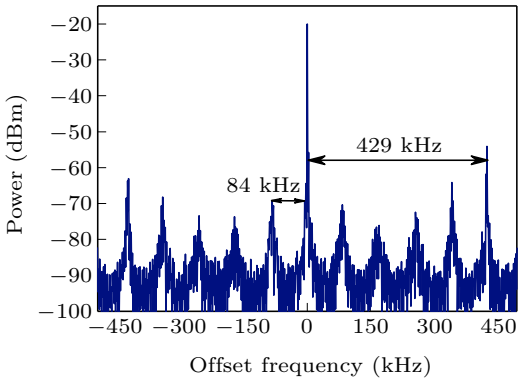


Fig. 3. Electrical spectrum of the OEO output (the resolution bandwidth is 0.75 kHz).

The performance of the proposed interrogation system in temperature measurement was evaluated. Part of the sensing arm was placed into a thermostatic water bath, and the length L of the optical fiber affected by the temperature variation was 106 cm. As shown in Fig. 4, the frequency of the OEO shifted toward a higher-frequency regime with increasing temperature. This is consistent with the theoretical analysis described in Eq. (5). The linear relationship between the frequency shift of the OEO and the temperature variation can be learned from Fig. 5. The temperature sensitivity and the correlation coefficient (R^2) are 35.35 MHz/°C and 0.99, respectively. To further

improve this sensitivity, L can be increased further. An appropriate decrease of the total dispersion D of the DCF would also help. Note that the frequency of the OEO changes from 7.8 GHz to 8.5296 GHz when the sensing head is moved from the test bench to the water bath. This is mainly due to the following two reasons. The first is the undesired disturbance and stretching of the MI arm during this movement. The second is the difference between room temperature and the water temperature. Nevertheless, when the optical fiber is fixed in the water bath at constant temperature, the OEO oscillates stably. Calibration is also required before the test.

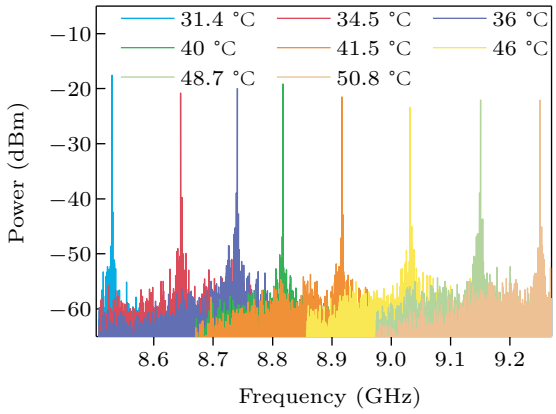


Fig. 4. OEO outputs at different temperatures.

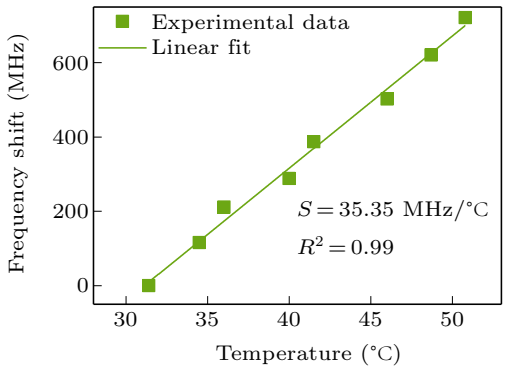


Fig. 5. Relationship between the temperature variation and the frequency shift of the OEO.

Next, the interrogation resolution and accuracy of the OEO-based interrogation system were investigated. Considering the use of the FRR and the corresponding mode spacing of 429 kHz, the theoretical interrogation resolution is 0.012 °C, which can be improved by decreasing the FSR Δf_{FRR} of the FRR when the sensitivity is fixed; however, Δf_{FRR} cannot be decreased arbitrarily due to mode competition of the OEO. This places an upper limit on the interrogation resolution. The interrogation accuracy is evaluated by measuring the stability of the OEO. As shown in Fig. 6, when the proposed OEO-based interrogation system operates in a room environment over 30 min, the measured frequency and power fluctuations are 2.88 MHz and 1.24 dB, respectively. Hence, the temperature interrogation accuracy corresponds to 0.08 °C. To improve this temperature interrogation accuracy further, the frequency fluctuation of the OEO should be minimized and an additional mechanism for further mode selection is required. Considering the OEO frequency tunable range of around 3 GHz (in this case) and the temperature sensitivity of 35.35 MHz/°C, the theoretical temperature interrogation range of the proposed interrogation system is around 84.9 °C. However, in practice this interrogation range can be improved by broadening the frequency tunable range of the OEO and the 3-dB bandwidth of the photoelectric devices (e.g., the 3-dB bandwidth of the PM).

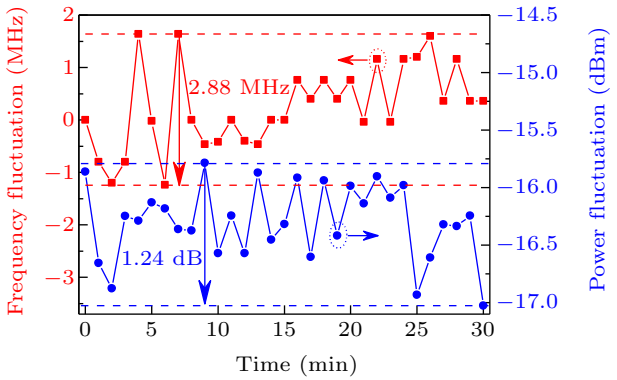


Fig. 6. Measured frequency fluctuation (red squares) and power fluctuation (blue circles) of the OEO.

A comparison of various temperature-sensing schemes and the interrogation approaches is shown in Table 1. Indeed, the interrogation resolution of our work should be improved compared with that in the work of Li *et al.*[4] However, unlike the wavelength interrogation scheme based on an OSA,[4,14,15] our work achieves wavelength-to-frequency mapping in the electrical domain, illustrating a potential method of high-speed interrogation that supports a wide linear interrogation range by avoiding overlapping of the measured spectrum.[18] Note that the interrogation speed reaches the MHz range when a digital signal processor unit is used.[19] Compared with a microwave photonics-based interrogation system using a VNA,[7,8] our work lowers the overall cost by avoiding the use of a VNA. In addition, compared with temperature measurement systems based on a Sagnac interferometer[13] or Mach–Zehnder interferometer,[17] a MI indeed provides a much higher sensitivity. The ultra-sensitive nature of a MI, in turn, implies that a MI is susceptible to undesired disturbance and the stability of the proposed interrogation system would be adversely affected to some extent. It is worth noting that when the sensing head is sensitive to other physical factors (e.g., refractive index, strain), the proposed OEO-based interrogation system can be used not only for temperature measurement but also the measurement of these physical factors.[20] Such an OEO-based interrogation system with high resolution and high speed would support practical applications such as bridge security monitoring and industrial machinery sensing.

Table 1. Comparison of various temperature sensing schemes.

Sensor head	Interrogation scheme	Speed	Sensitivity	Resolution (°C)	Range (°C)
Liquid-filled silica capillary tube[4]	Wavelength interrogation based on OSA	Slow	5.086 nm/°C	0.0039	25–55
Long period grating[14]	Wavelength interrogation based on OSA	Slow	1.316 nm/°C	0.0152	25–45
Thin fiber-based Sagnac interferometer (SI)[15]	Wavelength interrogation based on OSA	Slow	1.55 nm/°C	0.013	30–94.5
Fiber surface plasmon resonance[16]	Wavelength interrogation based on spectrometer	Fast	1.765 nm/°C	0.198	35–95
SI[13]	Frequency interrogation based on OEO	Fast	2.66 MHz/°C	0.096	16.5–61.5
Mach–Zehnder interferometer[17]	Frequency interrogation based on OEO	Fast	3.7 MHz/°C	0.015	25–75
Our work	Frequency interrogation based on OEO	Fast	35.35 MHz/°C	0.012	31.4–51.8 (can be extended to 84.9 °C)

4. Summary

In summary, we have demonstrated a MI interrogation system implemented in the electrical domain. The fundamental idea is wavelength-to-frequency mapping enabled by the OEO. With the applied external physical factors, the frequency of the OEO changes with the FSR shift of the MI. Operational feasibility is verified for temperature measurement, and the temperature sensitivity, interrogation resolution and interrogation accuracy are 35.35 MHz/°C, 0.012 °C, and 0.08 °C, respectively. The sensitivity can be improved by increasing the length of optical fiber affected by temperature. The interrogation resolution, although limited, is adjustable and can be improved by appropriately increasing the length of optical fiber constituting the FRR.

References

[1] Lee B 2003 *Opt. Fiber Technol.* **9** 57
[2] Liu L, Ning T, Zheng J, Pei L, Li J, Cao J, Gao X and Zhang C 2019 *Opt. Laser Technol.* **119** 105591
[3] Salloom H T, Jasim R I, Habubi N F, Chiad S S, Jadan M and Addasi J S 2021 *Chin. Phys. B* **30** 68505
[4] Li M, Feng B and Yin J 2019 *Chin. Phys. B* **28** 114201
[5] Zhao Y, Zhou A, Guo H, Zheng Z, Xu Y, Zhou C and Yuan L 2018 *J. Lightw. Technol.* **36** 993
[6] Chen X, He S, Li D, Wang K, Fan Y and Wu S 2016 *IEEE Sensors J.* **16** 349
[7] Huang J, Lan X, Song Y, Li Y, Hua L and Xiao H 2015 *IEEE Photon. Technol. Lett.* **27** 1398
[8] Dong H, Liu S, Yang L, Peng J and Cheng K 2018 *Sensors* **18** 3702
[9] Wang A, Xiao H, Wang J, Wang Z, Zhao W and May R G 2001 *J. Lightw. Technol.* **19** 1495
[10] Mora J, Ortega B, Díez A, Cruz J L, Andrés M V, Capmany J and Pastor D 2006 *J. Lightw. Technol.* **24** 2500
[11] Chen X, Yao J and Zeng F 2005 *IEEE Photon. Technol. Lett.* **17** 1390
[12] Zhu K, Ou H, Fu H, Remb E and He S 2008 *IEEE Photon. Technol. Lett.* **20** 1917
[13] Liu L, Gao H, Ning T, Pei L, Zheng J, Li J and Xu J 2020 *Opt. Laser Technol.* **123** 105951
[14] Jin W, Zhang L, Zhang X, Xu M, Bi W and Qi Y 2022 *Chin. Phys. B* **31** 14207
[15] Ge Q, Zhu J, Cui Y, Zhang G, Wu X, Li S, Wang H and Yu B 2022 *Opt. Commun.* **502** 127417
[16] Wei Y, Li L, Liu C, Hu J, Su Y, Wu P and Zhao X 2021 *Chin. Phys. B* **30** 100701
[17] Wang Y, Zhang J and Yao J 2016 *IEEE Photon. Technol. Lett.* **28** 1458
[18] Chen X, Yang S, Yun J, Wang K, Fu H and Chen N 2020 *IEEE Sensors J.* **20** 1202
[19] Yao J 2017 *J. Lightw. Technol.* **35** 3489
[20] Liu L, Ning T, Sun X, Xu J, Zhang J and You H 2021 *SPIE/COS Photonics Asia,* October 9–12, 2021, Nantong, China, 119010P